Therefore,

$$XPD_T(p) = (0.85 - 0.05 \log_{10} p)\, XPD_{rain}(p) \qquad (6.6\text{-}6)$$

This result, in conjunction with the CCIR estimation procedure for rain depolarization presented in Section 6.6.2.1.1, can be used to determine a total XPD distribution for a given set of link parameters.

6.6.4 Other Sources of Depolarization

6.6.4.1 Snow Depolarization. Snow depolarization occurs during both the winter and summer months. During the summer months snow exists above the 0°C isotherm. During winter, as the isotherm lowers, the thickness of the snow layer increases and the depolarization due to rain decreases.

In Canada (Hendry, et al-1976) tests using circularly polarized diversity radars at frequencies near 2.9 GHz (10.4 cm wavelength) and 16.7 GHz (1.8 cm wavelength) at an elevation angle of 3.2 degrees have diagnosed storms during both summer and winter. During June snow occurred during a storm from 2.6 to 8.2 km altitude and yielded a differential phase shift of 0.36 deg/km at 2.9 GHz. Winter data taken at 16.7 GHz gave more variable results of 0.16 to 1.17 deg/km for moderate to heavy snowstorms ranging in altitude from 70 m to 2.6 km. The mean value of differential phase shift was 0.69 deg/km at 16.7 GHz.

6.6.4.2 Multipath Depolarization. The cross-polarized pattern of a parabolic reflector antenna normally has its peak at small angles off-axis. This allows oblique indirect rays, which may be present on earth-space paths at low elevation angles, to produce a significant cross-polarized component. Measurements have been made on terrestrial links at 11 GHz (Watson, et al-1973) and 22 GHz (Turner-1973). The magnitude of the indirect signal reflected from the earth can be roughly estimated from the data in Lord and Oliver (1946) taken near 3 GHz.

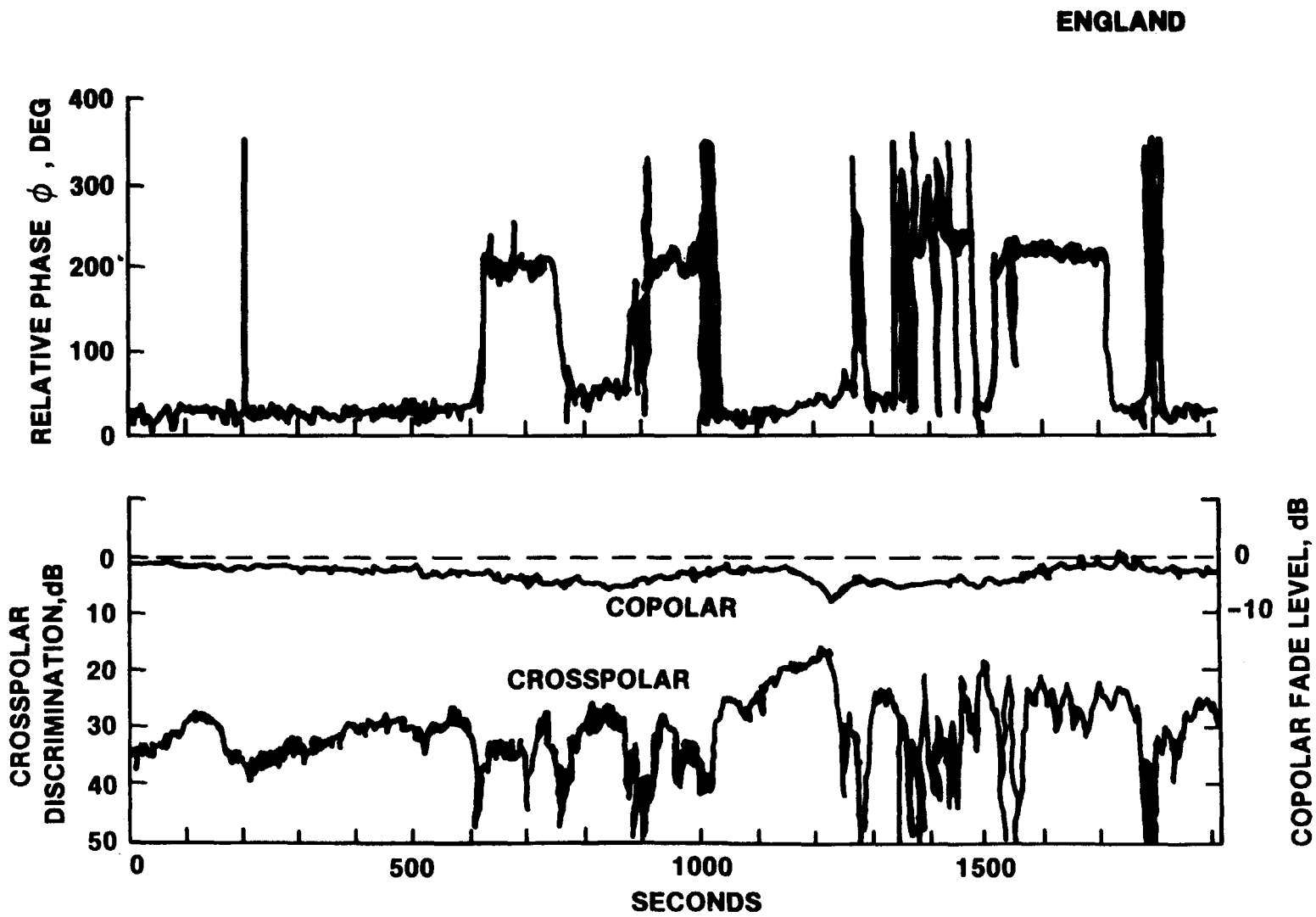

Figure 6.6-8. Phase, Copolar Fade and Crosspolar Discrimination for an Electrically Active Thunderstorm (15th July 1976)

6.6.4.3 Refractive Effects. Variations in the radio refractivity (dielectric constant of tropospheric layers) can cause rotation of the polarization plane of the rays refracting through the layers. This condition will occur for layers which are not perpendicular to the vertical plane containing the transmitter and receiver as described by LeFrancois, et al (1973).

6.6.5 Prediction of Depolarization Statistics

This section presents a summary of the procedure for developing a prediction of depolarization statistics, in the form of the cumulative distribution of XPD, for rain and ice-particle induced depolarization on a slant path. Figure 6.6-9 shows the methodology for developing the statistics. The XPD prediction requires the cumulative distribution of rain attenuation, either as measured or calculated from one of the methods described in Section 6.3.

The coefficients $\tilde{a}$ and $\tilde{b}$ are determined at each percent p from the CCIR procedure, Eq.'s 6.6-2 and 6.6-3, for the given frequency, elevation angle, and polarization tilt angle (STEP 1). The rain induced XPD is then determined from the coefficients and from the rain attenuation distribution by Eq. 6.6-1 (STEP 2). The contribution from ice particles is determined from the CCIR relationship, Eq. 6.6-6 (STEP 3).

The procedure is valid in the frquency range $8 \leq f \leq 35$ GHz. Outside of this frequency range, attenuation statistics are not useful in predicting XPD statistics. For frequencies below 8 GHz, relationships between XPD, point rain rate, and effective path length have been employed (see Oguchi-1977, Kobayashi-1977).

Long term XPD statistics obtained at one frequency and polarization tilt angle can be scaled (STEP 4) to another frequency and polarization tilt angle using the semi-empirical relation (CCIR Rpt. 564-3, 1986b),

$$XPD_2 = XPD_1 - 20 \log_{10}\left[\frac{f_2 \sqrt{1 - 0.484(1 + \cos 4\tau_2)}}{f_1 \sqrt{1 - 0.484(1 + \cos 4\tau_1)}} \right] \quad \text{for } 4 \le f_1, f_2 \le 30 \text{ GHz} \qquad (6.6\text{-}7)$$

where XPD_1 and XPD_2 are the XPD values not exceeded for the same percentage of time at frequencies f_1 and f_2 and polarization tilt angles τ_1 and τ_2, respectively. The above can be used to scale both rain and ice depolarization, since it has been observed that both phenomena have approximately the same frequency dependence at frequencies less than about 30 GHz.

Figure 6.6-10 show a sample calculation of the XPD procedure developed from cumulative attenuation statistics for Rosman, NC with the ATS-6 20 GHz satellite beacon. The attenuation statistics were obtained from the distribution extension technique described in Section 6.3. The curve labeled DEPOLARIZATION presents the XPD calculated from the procedure of Figure 6.6-9, with both the rain and rain + ice predictions shown.

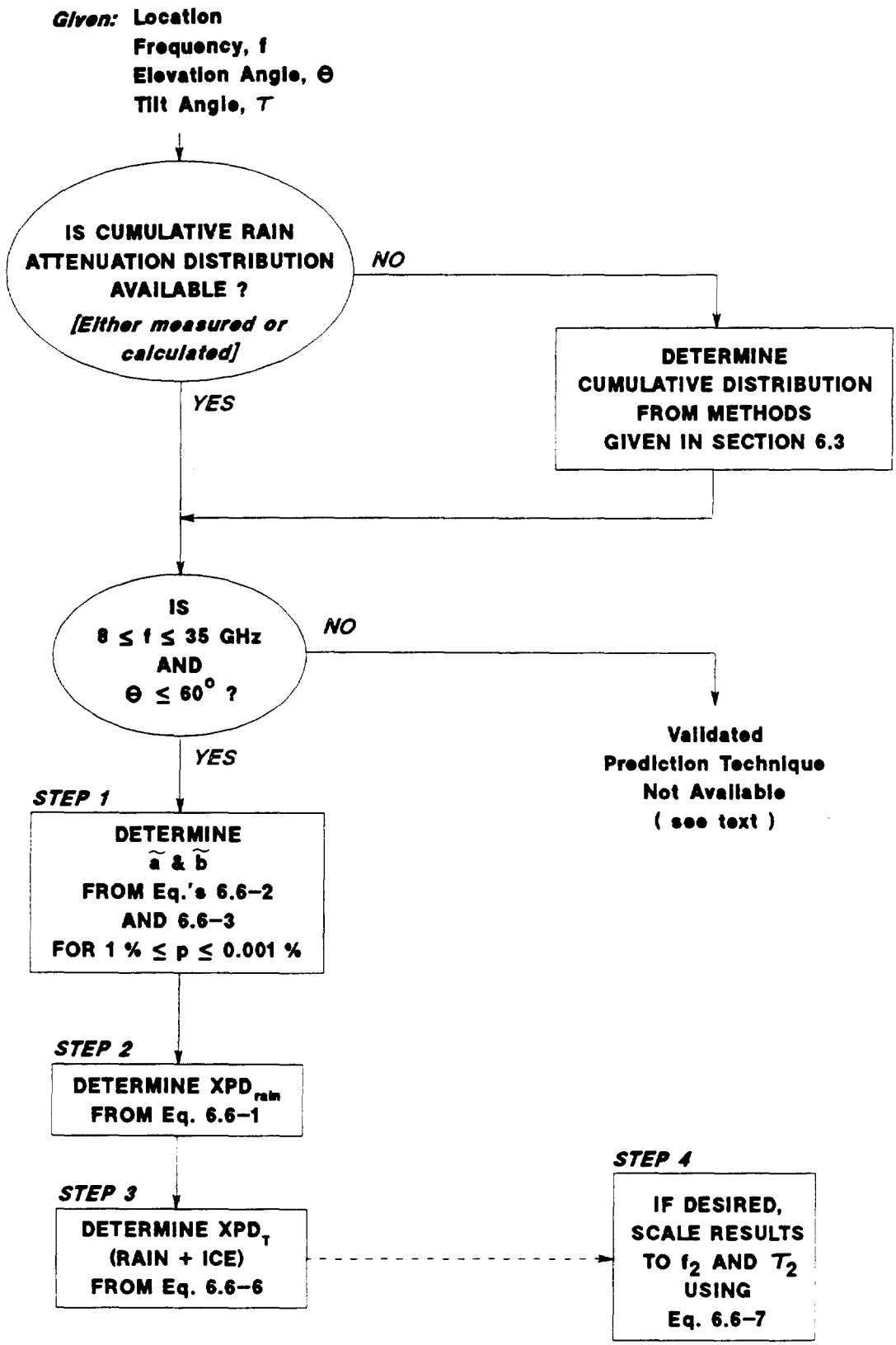

Figure 6.6-9. Technique for Prediction of Depolarization Statistics

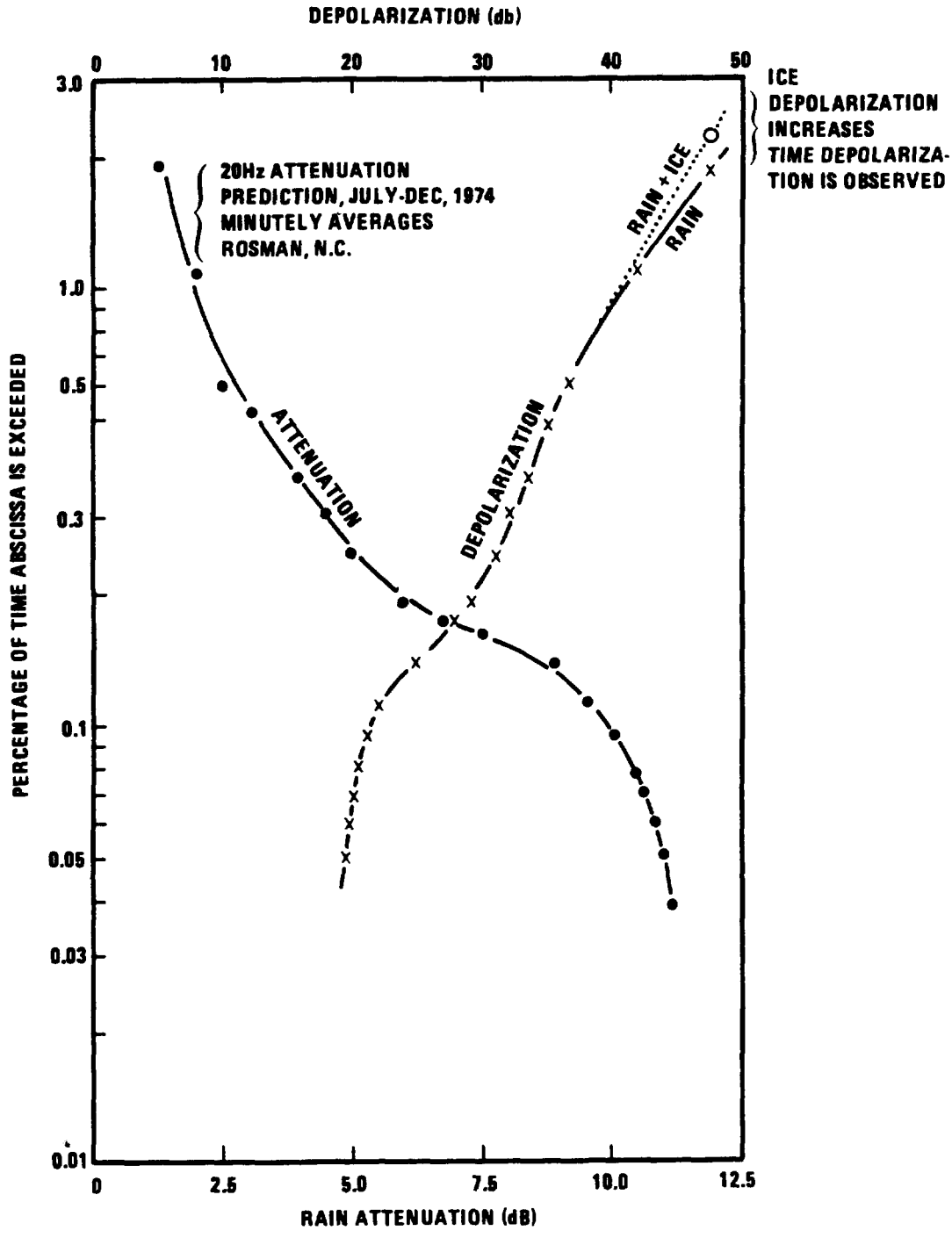

Figure 6.6-10. Attenuation and Depolarization Statistics for Rosman, N.E.

6.7 DISPERSION AND BANDWIDTH COHERENCE EFFECTS

When the dispersion of the propagating medium is sufficiently high, the phase and/or amplitude of wide-bandwidth transmissions may be selectively altered, causing a variation or reduction in the coherence bandwidth of the transmitted signal. Both tropospheric and ionospheric effects have been predicted and observed. This section reviews the analytical and experimental results for both tropospheric and ionospheric induced effects on radiowave paths operating above 10 GHz.

6.7.1 Tropospheric Effects on Bandwidth Coherence

6.7.1.1 Amplitude Variations

Theoretical estimates of the degradation of pulse shapes through rain have indicated that only minor effects are observed. The calculations (Crane-1967) indicated that pulse distortion does not become significant until total rain attenuations of the order of 100 dB are encountered. Since current link margins do not allow such high attenuations, the link will fail due to signal attenuation before pulse shape degradation affects transmission.

Amplitude variation with frequency becomes significant at frequencies in the vicinity of molecular absorption bands, such as the 50-70 GHz oxygen absorption band. The greatest dispersive effect would occur at the individual absorption lines which are quite narrow (Liebe -1955). However, due to the great path attenuation present at these frequencies, it is not likely they would be used for earth-space communications.

For rain the frequency dependence of the specific attenuation (db/km) is

$$\frac{\partial \alpha}{\partial f} = \frac{\partial (aR^b)}{\partial f} \; \alpha \left[\frac{1}{a} \frac{\partial a}{\partial f} + (\ln R) \frac{\partial b}{\partial f} \right] \qquad (6.7\text{-}1)$$

where, for example, for the frequency range from 8.5 to 25 GHz (Olsen et al-1977)

$$\frac{\partial a}{\partial f} = 1.02 \times 10^{-4} f^{1.42} \qquad (6.7\text{-}2)$$

$$\frac{\partial b}{\partial f} = -0.11 f^{-1.0779} \qquad (6.7\text{-}3)$$

For example, at 20 GHz and R = 25 mm/hr,

$$a = 5.93 \times 10^{-2}$$

$$b = 1.12$$

$$\frac{\partial a}{\partial f} = 7.18 \times 10^{-3}$$

$$\frac{\partial b}{\partial f} = -4.36 \times 10^{-3}$$

$$\alpha = 2.18 \text{ db/km}$$

so

$$\frac{\partial \alpha}{\partial f} = 0.23 \text{ dB/(km-GHz)}$$

or for a typical effective path length L_e = 6 km'

$$\frac{\partial(\alpha L_e)}{\partial f} = L_e \frac{\partial \alpha}{\partial f} = 1.38 \text{ dB/GHz}$$

6.7.1.1.1 Experimental Results. The ATS-6 beacons at 20 and 30 GHz were both capable of being modulated with ±180, 360, 540 and ±720 MHz sidetone signals. Typical selective fading events across the 1.44 GHz bands are shown in Figures 6.7-1 and 6.7-2, respectively (WEC-1975). These are four-second averages taken on day 270 of 1974 just before the onset of a fade event (230000Z) at the beginning of the fade event (232352Z), and before receiver lock was lost during the fade event (232428Z). Except for fade depths in excess of 20 dB, the accuracy of the attenuation measurements is +1 dB. These rain fade results, while representative of those taken at Rosman, do

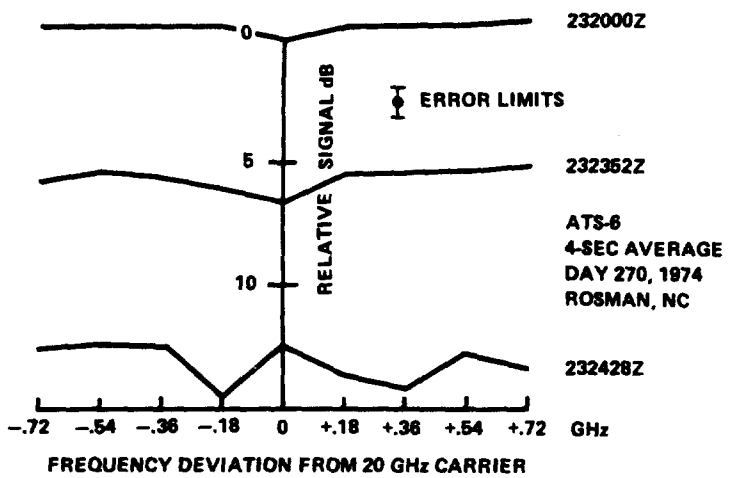

Figure 6.7-1. Selective Fading Near 20 GHz

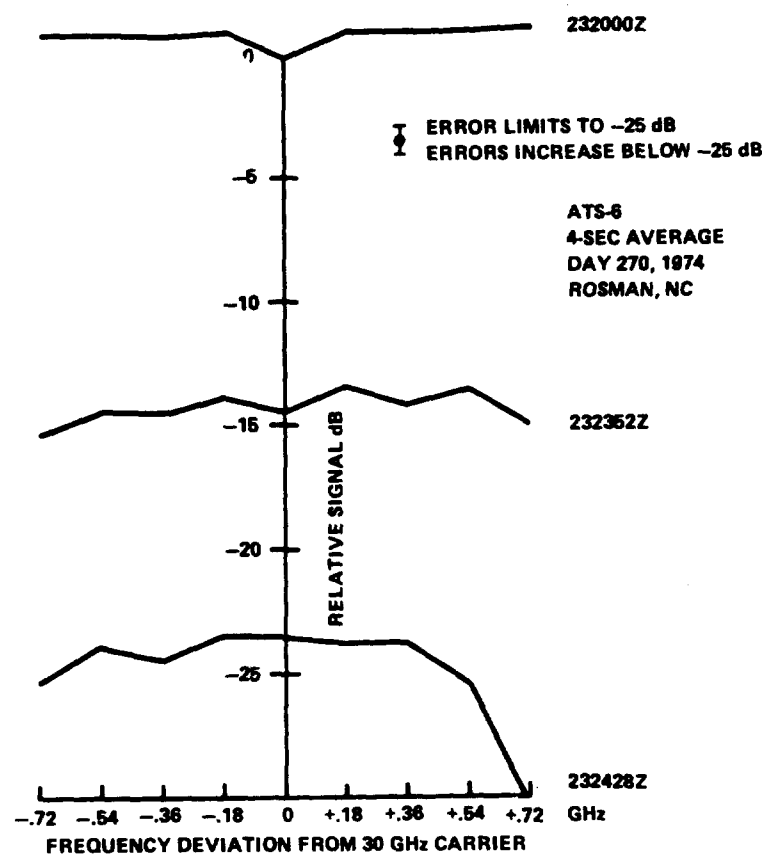

Figure 6.7-2. Selective Fading Near 30 GHz

not appear to be sufficiently accurate for deep fades because the signal levels approach the noise floor of the receiver. For one-minute averages, no measurable selective fading was observed (WEC-1975).

The cross-correlation of 4 and 6 GHz signals due to low angle fading in the Canadian arctic was found to be low (Strickland, et al-1977). During a 2.5 hour period on the day when the fading was most severe the correlation coefficient was 0.34 since the 6 GHz signal experienced 55% more fades than the 4 GHz signal. This would indicate significant dispersion was present, but the mechanism for this effect is tropospheric refraction and not rain. Frequency selective fading may be significant at low elevation angles.

6.7.1.2 Phase Variations. Phase measurements have not yielded significant results for frequencies above 10 GHz. The phase coherent sidetone signals on ATS-6 showed only minor variations across the 1.44 GHz bandwidths. These variations were most evident for the shorter (one and four second) averaging periods compared to the one-minute period (WEC-1975).

Phase measurements have been attempted for the one degree elevation angle satellites observed from the arctic (Strickland et al-1977). Unfortunately, no significant fade events occurred and no differential phase variations were recorded.

Phase effects are produced by the molecular absorption mechanism along with amplitude effects. Large values of phase dispersion would therefore be expected in the absorption bands.

6.7.2 Ionospheric Effects on Bandwidth Coherence

6.7.2.1 Amplitude Variations. Ionospheric attenuation at microwave frequencies is inversely proportional to the frequency squared (Flock, 1987) and is generally less than 0.001 dB at 15 GHz and an elevation angle $\theta = 90^{o}$. The variation is approximately related to cosecant θ. The attenuation is therefore usually less

than 0.01 dB above 10 GHz.

6.7.2.2 Phase Variations. The group delay due to the free electrons in the ionosphere is (Flock, 1987)

$$\Delta\tau = 40.3 \frac{N_e}{cf^2} = \frac{1.33 \times 10^{-7}}{f^2} N_e \quad \text{,sec} \qquad (6.7\text{-}4)$$

where N_e is the total electron content in electrons/m^2, c = 3×10^8 m/sec and f is in Hertz. This delay is equivalent to a phase delay (in radians)

$$\Delta\tau = \frac{\Delta\phi}{2\pi f} \qquad (6.7\text{-}5)$$

so that

$$\Delta\phi = (2\pi)(40.3) \frac{N_e}{cf} \qquad (6.7\text{-}6)$$

For a typical value of Ne = 10^{17} m^{-2}, the total phase delay at 11.7 GHz is only 7.21 radians. The frequency dependence of this is only

$$\frac{\partial(\Delta\phi)}{\partial f} = -\frac{2\pi(40.3)\ N_e}{cf^2}$$
$$= -6.2 \times 10^{-10} \text{ radian/Hertz}$$
$$= -0.62 \text{ radian/GHz}$$
$$= -35 \text{ degrees/GHz.}$$

For higher frequencies, the rate of change of phase with frequency decreases.

6.8 DOWNLINK NOISE AT EARTH STATIONS

6.8.1 Introduction

An Earth station observing a satellite at a high elevation angle

may be considered to be receiving sky noise from the antenna boresight direction. As the elevation angle of the satellite decreases, thermal noise emission from the Earth's surface will be increasingly observed in the antenna's sidelobes. This section reviews the sky noise component and its contribution to satellite communicaitons system performance.

Antenna noise is conveniently treated in terms of noise temperature, since the two paremeters are linearly related. In circuit theory the noise power, p_n, which is transferred to a matched load is

$$p_n = kTB \quad \text{watts} \tag{6.8-1}$$

where k is Boltzmann's constant, T is noise temperature in (degrees) Kelvin, and B is the bandwidth in Hertz. Thermal radiation from the gaseous atmosphere is given by the Rayleigh-Jeans longwave approximation to Plank's equation

$$p_n' = \frac{2kT}{\lambda^2} = 22.2kTf^2 \tag{6.8-2}$$

where f is the frequency in GHz. Note the ambiguity in the frequency dependence of the two relations. However, we will be considering noise temperature in its circuit theory usage so the difference is not of prime concern.

6.8.2 Clear Air Sky Noise

The thermal noise emission from a gas in thermodynamic equiblibrium, from Kirchhoff's law, must equal its absorption, and this equality must be true at all frequencies.

The noise temperature T_b in a given direction through the atmosphere (also called the brightness temperature) is given by radiative transfer theory (Waters-1976, Wulfsberg-1964)

$$T_b = \int_0^\infty T_m \gamma e^{-\tau} dl + T_\infty e^{-\tau_\infty} \tag{6.8-3}$$

where T_m is the ambient temperature, γ is the absorption coefficient, and τ is the optical depth to the point under consideration. In radio engineering terms

$$\tau = 4.343\ A \qquad dB \tag{6.8-4}$$

where A is the apsorption over the path in question, in dB. For frequencies above 10 GHz, the second term on the righthand side of Eq. (6.8-3) reduces to 2.7 K, the cosmic background component, unless the Sun is in the antenna beam, as illustrated in Figure 6.8-1.

For an isothermal atmosphere (T_m constant with height), substituting $\gamma dl = d\tau$ in Eq. (6.8-3) yields

$$T_b = T_m(1 - e^{\tau}) = T_m\left(1 - 10^{-\frac{A}{10}}\right) \qquad K \tag{6.8-5}$$

where A is again atmospheric absorption in dB. The value of T_m taken in Eq. (6.8-4) ranges from 260 to 280 K. One relationship used to determine a value of T_m from surface measured temperature is (Wulfsberg-1964)

$$T_m = 1.12\ T_s - 50 \qquad K \tag{6.8-6}$$

where T_s is the surface temperature in K.

Noise temperature (or brightness temperature) curves for 3, 7.5, and 17 g/m^3 surface water vapor content, with the US Standard Atmosphere for the two lower values and the Tropical Atmosphere for the highest value, have been published by Smith (1982) and reproduced in CCIR Report 720-2(CCIR-1986h). Examples for an average humidity state (7.5 g/m^3 at the surface) are reproduced as Figures 6-8-2 and 6.8-3.

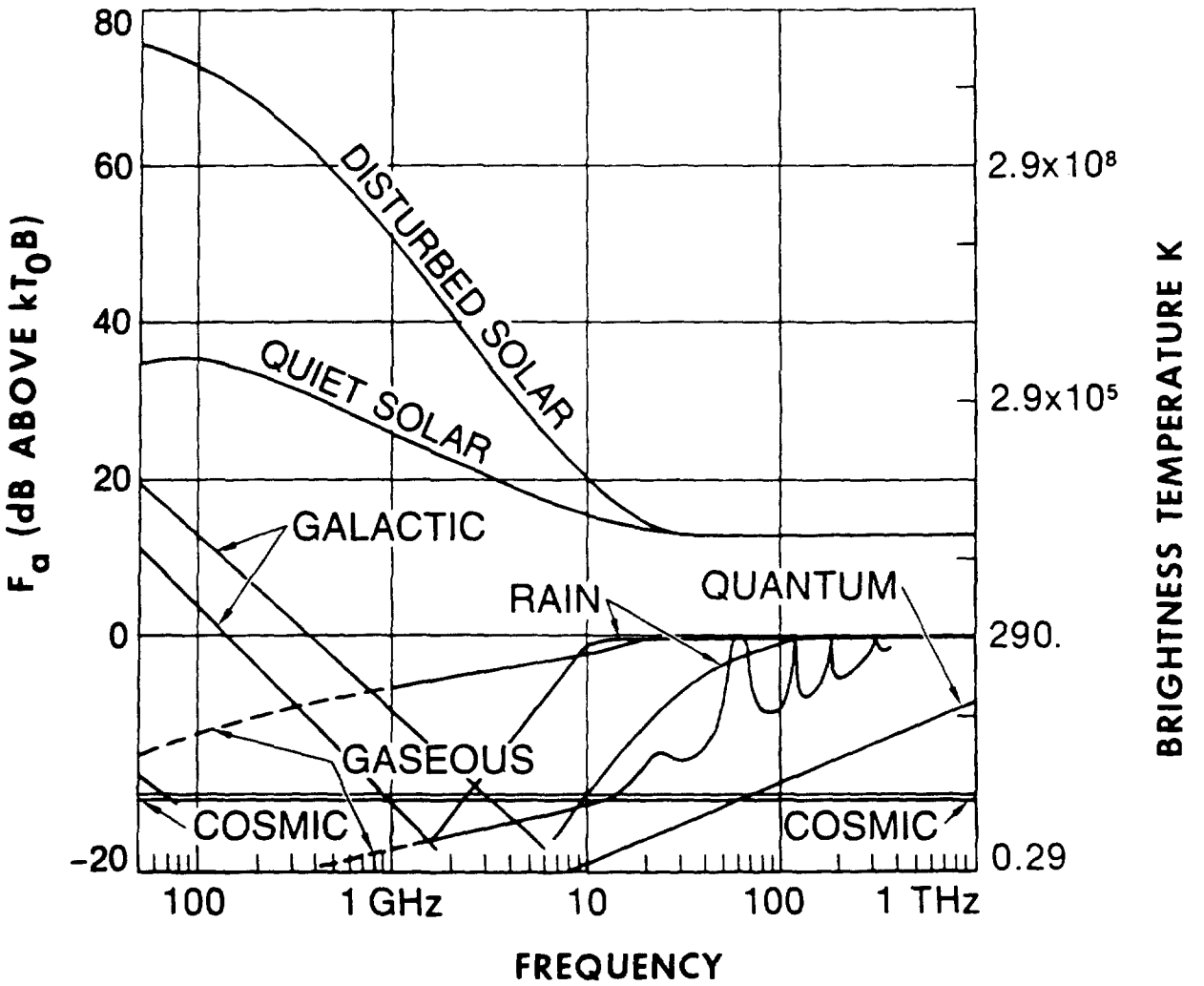

Figure 6.8-1. Noise Factor and Brightness Temperature from Natural Sources observed on Satellite Downlinks [Source: Spaulding and Hagn - 1978]

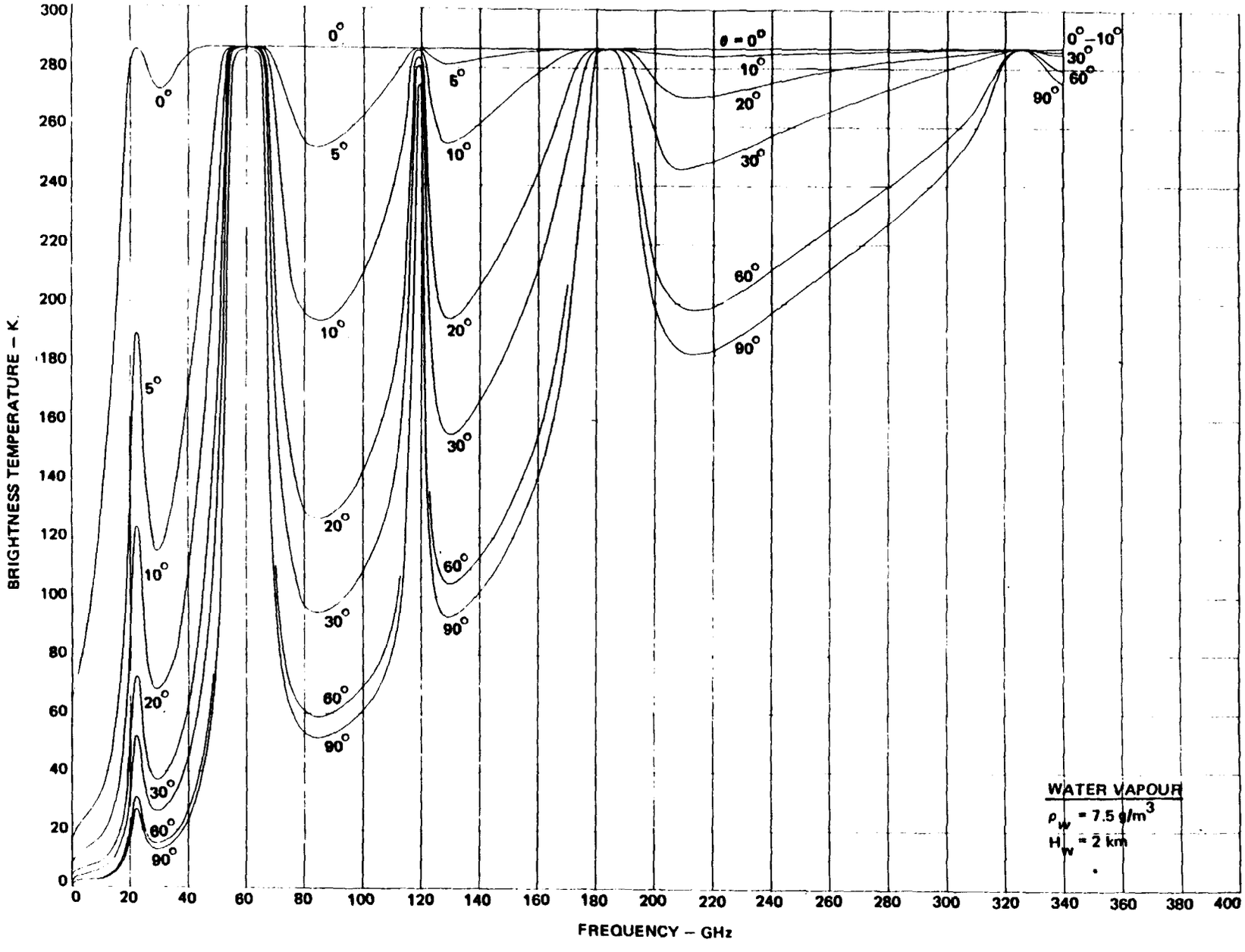

Figure 6.8-2. Brightness Temperature (Clear Air) for a Water Vapor Concentration of 7.5 g/m^3, 1 to 350 GHz. [Smith - 1982]

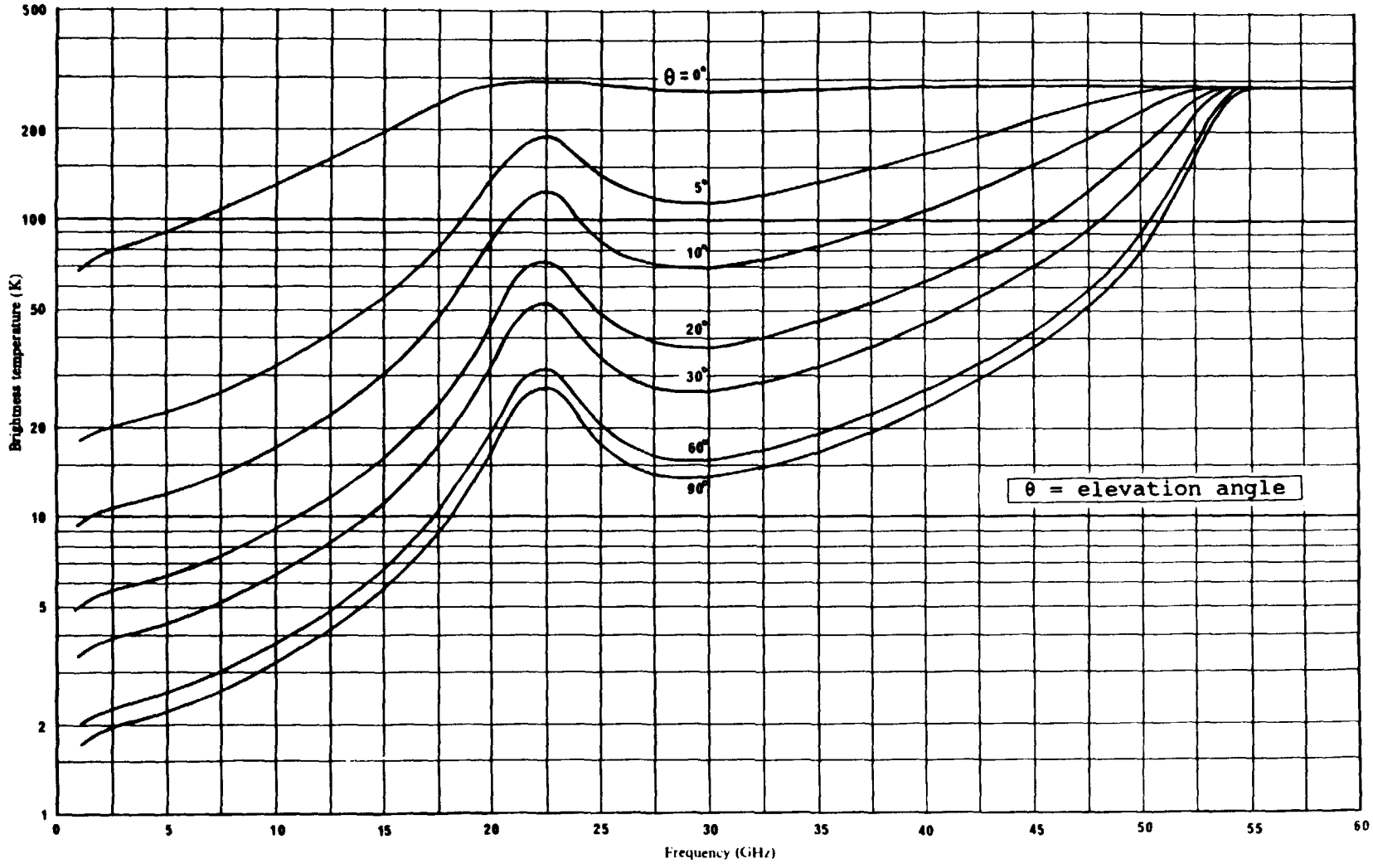

Figure 6.8-3. Brightness Temperature (Clear Air) for a Water Vapor Concentration of 7.5 g/m^3, Expanded Scale, 1 to 60 GHz. [Smith - 1982]

6.8.3 Sky Noise Due to Rain

Kirchhoff's law applies to noise emission from rain as well as from atmospheric gases, but only to the absorption component of the rain attenuation and not to the scattered component. The scattered component increases with frequency, so that while Eq. (6.8-5) may be appropriate at 10 GHz, it will give too high a value at 70 GHz.

Values of T_s due to rain may be estimated from the rain attenuation calculation techniques presented in Section 6.3. For example, to compute the cumulative statistics of T_s, first compute the cumulative attenuation statistics due to rain, and then use Eq. 6.8.5 to convert attenuation to apparent sky noise temperature. An example of this process has been done for Rosman, NC at 20 GHz. The results are given in Table 6.8-1.

The sky noise temperature (see last column of Table 6.8-1) will degrade the overall system noise figure of the receiver system. For example, for a receiver with a 4 dB noise figure, the resultant noise figure for the rain rate corresponding to 0.01% of the year will be 5.4 dB, i.e., an increase of 1.4 dB.

6.8.4 Sample Calculations

Two illustrative examples of application of the sky noise relationships for clear air and for rain are presented below.

Example 1. A land mobile satellite system downlink is to operate at 20 GHz with a service reliability of 95 % of the time. The receiver system noise temperature, exclusive of antenna noise, is 100 K. The elevation angle to the satellite is 60°. The median surface humidity is estimated at 7.5 g/m^3. What is the required propagation margin?

From Figure 6.8-3 we read T = 20 K for the parameters given above. For the worst 5 % of the time we arbitrarily double this value to T = 40 K.

The gaseous attenuation for the link can be determined from the

Table 6.8-1. Cumulative Statistics of Sky Temperature Due to Rain for Rosman, N.C. at 20 GHz. T_m = 275 K.

PERCENT OF YEAR	POINT RAIN RATE VALUES	AVERAGE RAIN RATE	TOTAL RAIN ATTENUATION*	SKY NOISE TEMPERATURE†
0.001	102 mm/hr	89 mm/hr	47 dB	275 K
0.002	86	77	40	275
0.005	64	60	30	275
0.01	49	47	23	274
0.02	35	35	16	269
0.05	22	24	11	252
0.1	15	17	7	224
0.2	9.5	11.3	4.6	180
0.5	5.2	6.7	2.6	123
1.0	3.0	4.2	1.5	82
2.0	1.8	2.7	0.93	53

NOTES:

* At 20 GHz the specific attenuation A = 0.06 $R_{ave}^{1.12}$ dB/km and for Rosman, N.C. the effective path length is 5.1 km to ATS-6.

† For a ground temperature of 17°C = 63°F the T_m = 275 K.

CCIR estimation procedure given in Section 6.2.3. The resulting total (oxygen + water vapor) attenuation is found as

$$A_g = 0.34 \text{ dB}$$

Doubling the value for the worst 5 % of the time, the attenuation is 0.68 dB.

At the 95 % reliability level, attenuation caused by rain may be ignored, since rain occurs only 2-3 % of the total time for most regions.

The propagation margin is then computed as follows:

Decrease in signal level = 0.68 dB.
Increase in noise temperature = 10 log[(100 + 40 +2.7)/100]
= 1.54 dB
Required propagation margin = 0.68 + 1.54 = 2.22 dB.

Note that for this case the sky noise increase contribution is more than double the contribution due to the decrease in signal level to the total margin required.

Example 2. A satellite system is to operate in the fixed service with a downlink at 20 GHz. The required service reliability is 99.99 % of the time. The 0.01 % of the time rain rate has been measured to produce an attenuation of 30 dB in the direction of the satellite. The reciever system noise temperature, exclusive of antenna noise, is 300 K. What is the required propagation margin?

The clear air component is assumed to be the 95 % value from example 1, i.e. T = 40 K, A = 0.68 dB.

The sky noise increase due to a rain attenuation of 30 dB is determined from Eq. (6.8-5)

$$T_r = 280(1 - 10^{-30/10}) = 279.7 \text{ K}$$

The propagation margin is then computed as follows:

Decrease in signal level = 30 + 0.68 = 30.68 dB.
Increase in noise temperature = 10 log[(279.7 + 300)/300]
= 2.86 dB.
Required propagation margin = 30.68 + 2.86 = 33.54 dB.

For this example the signal level decrease is the predominate factor in the margin requirement.

Note that the reliability criterian plays a significant role in propagation margins for the two above examples (2.22 vs 33.54 dB). The relative difference in receiver noise temperature, however, also accounts for the greater importance of noise over attenuation in the first example.

6.8.5 Sky Noise Due to Clouds, Fog, Sand and Dust. The major contributor to the sky noise temperature is the medium with the highest attenuation. Generally, clouds will present higher attenuations than fog, sand or dust. For example, for cumulus clouds with no precipitation the water density will be approximately 0.5 g/m^3. For the Rosman example described earlier (20 GHz),

$$A = K_c \rho_l t_c \csc \theta \qquad (6.8\text{-}7)$$

where t_c is the thickness of the clouds (typically 2 kilometers). Using typical numbers

$A = (0.4 \text{ dB } m^3/\text{gm km}) (0.5 \text{ gm}/m^3) (2 \text{ km}) \csc (47^o)$
$= 0.55 \text{ dB}$

The corresponding sky noise contribution is then

$$T_s = T_{mc} [1 - 10^{-(0.55/10)}]$$

With T_{mc} equal to the temperature of the cloud (i.e., T_{mc} =

$0^{o}C$ = 273 K), T_s is 32 K. Clearly, at 20 GHz, rain represents a much more significant contributor to the sky noise temperature than clouds.

6.8.6 Total Sky Noise Temperature Arising from Several Contributors. The sky noise temperatures from several sources do not add linearly. Rather, the attenuation from each contributor must be added and the total result substituted into the sky noise versus attenuation relation. For example, for the Rosman ground station observing the ATS-6, the clear air attenuation is 1.2 dB yielding a T_s (clear air) = 66 K. From Table 6.8-1 for 0.2% of the year (105 minutes) the rain induced sky temperature due to clear air and rain is 203 K which is significantly less than the sum of each contributor (246 K). During rain conditions the cloud contributions should also be added, but these will generally be even a smaller contribution than the clear air attenuation.

6.8.7 Extraterrestrial Sources of Sky Noise

6.8.7.1 Solar Noise. The sun generates very high noise levels when it is collinear with the Earth station-satellite path. For geostationary satellites, this occurs near the equinoxes, for a short period each day. The power flux density generated by the sun is given as a function of frequency in Figure 6.8-4 (Perlman, et al-1960). Above about 20 GHz, it is practically constant at -188 dBW/Hz-m^2 for "quiet sun" conditions.

Reception of solar noise can be viewed as an equivalent increase in the antenna noise temperature by an amount T_s. T_s depends on the relative magnitude of the antenna beamwidth compared with the apparent diameter of the sun (0.48^{o}), and how close the sun approaches the antenna boresight. The following formula, after Baars (1973), gives an estimate of T_s (in Kelvins) when the sun, or another extraterrestrial noise source, is centered in the beam.

$$T_s = \frac{1 - e^{-\left(\frac{D}{1.2\theta}\right)^2}}{f^2D^2} \log^{-1}\left(\frac{S + 250}{10}\right) \qquad (6.8\text{-}9)$$

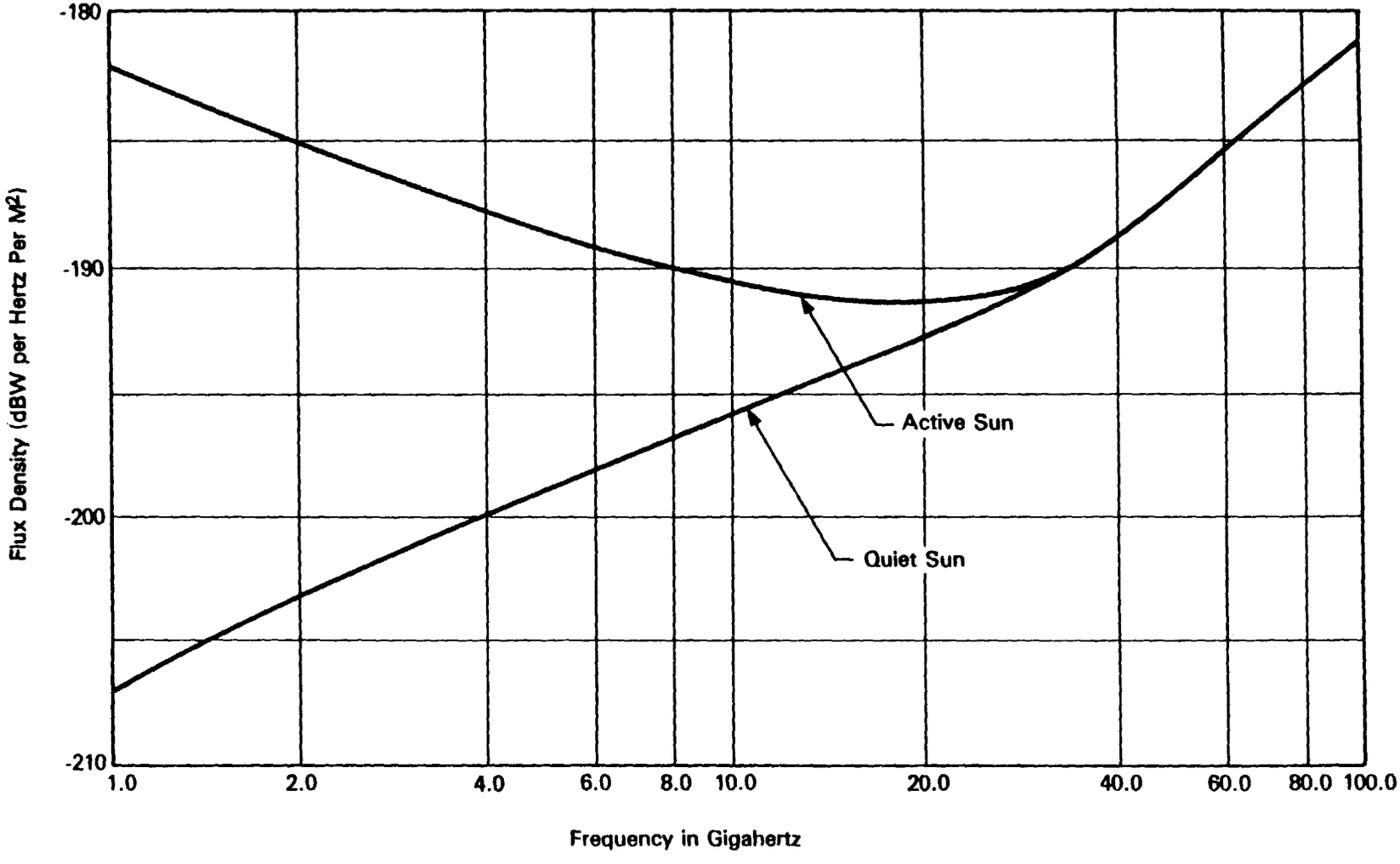

Figure 6.8-4. Values of Noise from Quiet and Active Sun

where D = apparent diameter of the sun, deg
f = frequency, GHz
S = power flux density, dBw/Hz-m^2
θ = antenna half-power beamwidth, deg

For an Earth station operating at 20 GHz with a 2 m diameter antenna (beamwidth about 0.5^o), the maximum increase in antenna temperature that would be caused by a ("quiet") sun transit is about 8100 K, according to the formula.

The sun's flux has been used extensively for measuring tropospheric attenuation. This is done with a sun-tracking radiometer, which monitors the noise temperature of an antenna that is devised to automatically remain pointed at the sun.

6.8.7.2 Lunar Noise. The moon reflects solar radio energy back to the Earth. Its apparent size is approximately 1/2 degree in diameter, like the sun. The noise power flux density from the moon varies directly as the square of frequency, which is characteristic of radiation from a "black body." The power flux density from the full moon is about -202 dBW/Hz-m^2 at 20 GHz. The maximum antenna temperature increase due to the moon, for the 20 GHz 2m antenna considered earlier, would be only about 320K. Because of the phases of the moon and the ellipticity of its orbit, the apparent size and flux vary widely, but in a regular and predictable manner. The moon has been used in measuring Earth station G/T (Johannsen and Koury-1974).

6.8.7.3 Radio Stars. The strongest radio stars are ten times weaker than the lunar emission. The strongest stars (Wait, et al-1974) emit typically -230 dBW/Hz-m^2 in the 10 to 100 GHz frequency range. Three of these strong sources are Cassiopeia A, Taurus A and Orion A. These sources are sometimes utilized for calibration of the ground station G/T. During the calibrations the attenuation due to the troposphere is usually cancelled out by comparing the sky noise on the star and subtracting the adjacent (dark) sky noise.

6.9 UPLINK NOISE IN SATELLITE ANTENNAS

6.9.1 Components of Uplink Noise

The earth viewing (uplink) antenna of an orbiting satellite typically includes only a portion of the earth's surface within its half-power beamwidth. The observed noise is a complex function of atmospheric and surface temperature, elevation angle, frequency, and antenna gain (see, for example, Report 720-2, CCIR-1986h). A major factor in the observed noise temperature is the fraction of land (high brightness temperature) to sea (low brightness temperature) in the main antenna beam. This factor is illustrated in Figure 6.9-1, which shows the variation in antenna temperature at a geostationary satellite using an earth-coverage antenna with a gaussian beam as it is moved around the geostationary orbit (Njoku and Smith - 1985). At the lowest frequency (1 GHz) the variation with subsatellite longitude is entirely due to the land/sea fraction. As the frequency increases, the effects of the atmosphere come into play. The brightness temperature values used to compute Figure 6.9-1 are given in Figure 6.9-2, as a function of frequency and location (latitude), and they may be used for computation of more specialized satellite antenna coverage systems.

6.9.2 Sample Calculation

Consider a satellite in geostationary orbit that has a spot beam directed at the Washington D.C. area such that 60 % of the area within the 3 dB contour is land and 40 % is sea. The great-circle distance from the sub-satellite point to the center of the spot beam is 60^{o} in equivalent latitude and the frequency is 40 GHz. What is the uplink antenna noise temperature at the satellite?

The satellite antenna noise temperature T_s may be approximated from Figure 6.9-2. The land portion will have a brightness temperature of 275 K, and the sea portion will be 185 K. Therefore

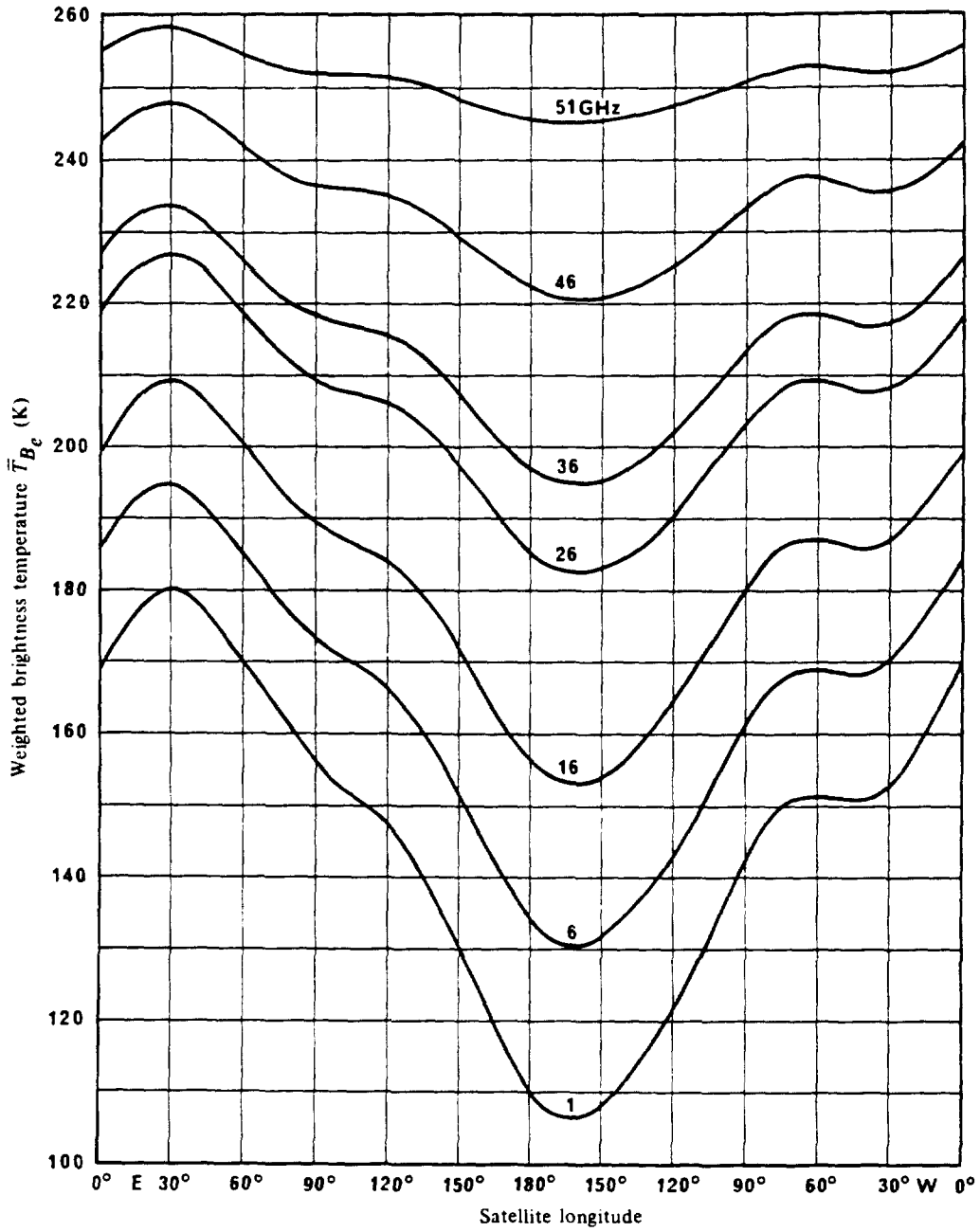

Curves are for US Standard Atmosphere with 7.5 g/cm^3 water vapor and 50 % cloud cover. The Earth Coverage antenna pattern is given by

$$G(\phi) = -3\left(\frac{\phi}{8.715}\right)^2 \text{ dB} \quad \text{for } 0 \leq \phi \leq 8.715$$

where ϕ is the angle off of boresight. (Njoku and Smith - 1985)

Figure 6.9-1. Weighted Brightness Temperature of the Earth as a Function of Longitude, Viewed from Geostationary Orbit at Frequencies between 1 and 51 GHz.